atmosphere

MDPI

Article

A Decade of Poland-AOD Aerosol Research Network Observations

Krzysztof M. Markowicz [1,*], Iwona S. Stachlewska [1], Olga Zawadzka-Manko [1], Dongxiang Wang [1], Wojciech Kumala [1], Michal T. Chilinski [2], Przemyslaw Makuch [3], Piotr Markuszewski [3], Anna K. Rozwadowska [3], Tomasz Petelski [3], Tymon Zielinski [3], Michal Posyniak [4], Jacek W. Kaminski [4], Artur Szkop [4], Aleksander Pietruczuk [4], Bogdan H. Chojnicki [5], Kamila M. Harenda [5], Patryk Poczta [5], Joanna Uscka-Kowalkowska [6], Joanna Struzewska [7], Malgorzata Werner [8], Maciej Kryza [8], Anetta Drzeniecka-Osiadacz [8], Tymoteusz Sawinski [8], Arkadiusz Remut [8], Miroslaw Mietus [9,10], Krzysztof Wiejak [9], Jacek Markowicz [11], Livio Belegante [12] and Doina Nicolae [12]

1 Institute of Geophysics, Faculty of Physics, University of Warsaw, 00-927 Warsaw, Poland; Iwona.Stachlewska@fuw.edu.pl (I.S.S.); Olga.Zawadzka@fuw.edu.pl (O.Z.-M.); Dongxiang.Wang@fuw.edu.pl (D.W.); Wojciech.Kumala@fuw.edu.pl (W.K.)
2 Faculty of Biology, University of Warsaw, 00-927 Warsaw, Poland; mich@igf.fuw.edu.pl
3 Institute of Oceanology, Polish Academy of Sciences, 81-712 Sopot, Poland; makuch@iopan.pl (P.M.); pmarkusz@iopan.pl (P.M.); ania@iopan.pl (A.K.R.); petelski@iopan.pl (T.P.); tymon@iopan.pl (T.Z.)
4 Institute of Geophysics, Polish Academy of Sciences, 00-901 Warsaw, Poland; mpos@igf.edu.pl (M.P.); jkaminski@ecoforecast.net (J.W.K.); aszkop@igf.edu.pl (A.S.); alek@igf.edu.pl (A.P.)
5 Department of Ecology and Environmental Protection, Faculty of Environmental and Mechanical Engineering, Poznan University of Life Sciences, 60-637 Poznan, Poland; bogdan.chojnicki@up.poznan.pl (B.H.C.); kamila.harenda@up.poznan.pl (K.M.H.); patryk.poczta@puls.edu.pl (P.P.)
6 Department of Meteorology and Climatology, Faculty of Earth Sciences and Spatial Management, Nicolaus Copernicus University, 87-100 Torun, Poland; joannauk@umk.pl
7 Faculty of Building Services, Hydro and Environmental Engineering, Warsaw University of Technology, 00-661 Warsaw, Poland; joanna.struzewska@pw.edu.pl
8 Faculty of Earth Sciences and Environmental Management, University of Wroclaw, 50-137 Wroclaw, Poland; malgorzata.werner@uwr.edu.pl (M.W.); maciej.kryza@uwr.edu.pl (M.K.); anetta.drzeniecka-osiadacz@uwr.edu.pl (A.D.-O.); tymoteusz.sawinski@uwr.edu.pl (T.S.); arkadiusz.remut@uwr.edu.pl (A.R.)
9 Department of Meteorology and Climatology, Faculty of Oceanography and Geography, University of Gdansk, 80-309 Gdansk, Poland; Miroslaw.Mietus@imgw.pl (M.M.); klimat@ug.edu.pl (K.W.)
10 Institute of Meteorology and Water Management, National Research Institute, 03-301 Warsaw, Poland
11 Aerosol and Radiation Observatory SolarAOT, 38-100 Strzyzow, Poland; jmarko90@gmail.com
12 Remote Sensing Department, National Institute of Research and Development for Optoelectronics INOE 2000, 077125 Magurele, Romania; belegantelivio@inoe.ro (L.B.); nnicol@inoe.ro (D.N.)
* Correspondence: kmark@igf.fuw.edu.pl; Tel.: +48-(0)-225532047

Abstract: The Poland-AOD aerosol research network was established in 2011 to improve aerosol–climate interaction knowledge and provide a real-time and historical, comprehensive, and quantitative database for the aerosol optical properties distribution over Poland. The network consists of research institutions and private owners operating 10 measurement stations and an organization responsible for aerosol model transport simulations. Poland-AOD collaboration provides observations of spectral aerosol optical depth (AOD), Ångstrom Exponent (AE), incoming shortwave (SW) and longwave (LW) radiation fluxes, vertical profiles of aerosol optical properties and surface aerosol scattering and absorption coefficient, as well as microphysical particle properties. Based on the radiative transfer model (RTM), the aerosol radiative forcing (ARF) and the heating rate are simulated. In addition, results from GEM-AQ and WRF-Chem models (e.g., aerosol mass mixing ratio and optical properties for several particle chemical components), and HYSPLIT back-trajectories are used to interpret the results of observation and to describe the 3D aerosol optical properties distribution. Results of Poland-AOD research indicate progressive improvement of air quality and atmospheric turbidity during the last decade. The AOD was reduced by about 0.02/10 yr (at 550 nm), which corresponds to positive trends in ARF. The estimated clear-sky ARF trend is 0.34 W/m^2/10 yr

Citation: Markowicz, K.M.; Stachlewska, I.S.; Zawadzka-Manko, O.; Wang, D.; Kumala, W.; Chilinski, M.T.; Makuch, P.; Markuszewski, P.; Rozwadowska, A.K.; Petelski, T.; et al. A Decade of Poland-AOD Aerosol Research Network Observations. *Atmosphere* **2021**, *12*, 1583. https://doi.org/10.3390/atmos12121583

Academic Editors: Magdalena Reizer, Jerzy Sowa and Zbigniew Nahorski

Received: 1 November 2021
Accepted: 25 November 2021
Published: 27 November 2021

and 0.68 W/m^2/10 yr, respectively, at TOA and at Earth's surface. Therefore, reduction in aerosol load observed in Poland can significantly contribute to climate warming.

Keywords: aerosol; aerosol optical depth; aerosol optical properties; Poland-AOD; radiometer; lidar; sun photometer

1. Introduction

Aerosol particles have a significant effect both on the climate system and on air quality [1]. Aerosol particles may have a warming or cooling effect on climate, depending on their physical and chemical properties and reflectance of the Earth's surface [1]. Therefore, the aerosol–climate effect on a regional scale can be completely different from the global one [2]. In addition, the regional influence of aerosols on climate and weather tends to be stronger than their global average impact due to their relatively short atmospheric lifetimes and inhomogeneity in sources, transport, and deposition [3]. On the regional scale, aerosol particles may significantly affect air quality due to high emissions and specific weather and topographic conditions [4].

Information on aerosol particle properties can be obtained from ground-based aerosol networks. The aerosol research networks are constantly growing. One of the most dynamic is the AErosol RObotic NETwork (AERONET, [5]) operated by the National Aeronautics and Space Administration (NASA) and PHOTONS (PHOtométrie pour le Traitement Opérationnel de Normalisation Satellitaire; University of Lille, CNES, and CNRS-INSU), which focuses on monitoring aerosol columnar properties by using CIMEL sun photometers. Direct and indirect retrieval provides information on the spectral aerosol optical depth (AOD), single scattering albedo (SSA), asymmetry parameter, particle size distribution, and refractive index, as well as precipitable water. The Maritime Aerosol Network is a component of AERONET, which observes AOD and AE over the ocean using handheld Microtops sun photometers [6]. The international network SKYNET (SKYrad NETwork [7]) focuses on aerosols and their interaction with clouds and solar radiation. It comprises approximately 60 stations, which are located mainly in Asia and Europe. The standard instrument in this network is the PREDE sun photometer, which can measure and retrieve the same optical and microphysical properties as the CIMEL instrument.

The lidar networks also measure the profiles of aerosol optical properties. The European Aerosol Research Lidar Network (EARLINET) [8], was established in 2000 and currently comprises 32 stations located mainly in Europe. It delivers high-quality data, including profiles of wavelength-resolved particle backscattering, extinction coefficient, and depolarization ratio, based on observations from the Raman and Mie lidars. The NASA Micro-Pulse Lidar Network (MPLNET, [9]), established in the 1990s, includes about 80 sites equipped with MPL eye-save lidars systematically upgraded and currently included with polarization. The AD-Net is an Asian lidar network [10], which focuses on mineral dust and anthropogenic pollution observations using the Raman lidar and the high spectral resolution lidar (HSRL). The lidar networks contribute to the World Meteorological Organization (WMO) Global Atmospheric Watch Aerosol Lidar Observation Network (GALION).

A more comprehensive range of aerosol topics is being researched by the National Oceanic and Atmospheric Administration (NOAA) Earth System Research Laboratory (ESRL)'s Global Monitoring Division (GMD). They are focused on global aerosol radiative forcing (ARF) and monitoring aerosol optical properties at 30 sites worldwide. Other examples of regional networks are CARSNET (China Aerosol Remote Sensing NETwork, [11]) and NACCM (National Aerosol Chemical Composition Monitoring Network of China, [12]).

During the past several decades, large infrastructures have emerged based on several network activities. In Europe, the Aerosol, Clouds, and Trace Gases Research Infrastructure (ACTRIS, https://actris.eu, accessed on 24 November 2021) delivers observations with

state-of-the-art equipment to obtain high-quality data and information on aerosol, clouds, and short-lived atmospheric constituents as well as on the physicochemical processes by combining the efforts of the EARLINET as mentioned earlier, CLOUDNET (Development of European pilot network of stations for observing cloud profiles), EUSAAR (European Supersites for Atmospheric Aerosol Research), and EUROCHAMP (Integration of European Simulation Chambers for Investigating Atmospheric Processes) infrastructures. Another large-scale initiative is called SARGAN (in situ Aerosol GAW Network) that includes 290 stations focused on aerosol properties [13].

Ten years ago in Poland, the infrastructure for studying aerosol–climate interactions was poorly developed. At that time, there was only one AERONET and EARLINET site in Belsk, in Central Poland. In addition, there was a network of monitoring stations of Poland's Chief Inspectorate of Environmental Protection (GIOS), which focused on air quality surface observations. Poland is one of the most polluted countries in the EU [14], with significant spatial variability of anthropogenic emissions and natural aerosol sources also affected by the long-range transport of aerosol [15–18]. Therefore, we have a strong motivation to establish the PolandAOD research network to expand knowledge on aerosol physical processes, optical and microphysical properties, and the impact of particles on the climate system.

2. Network Overview

The Poland-AOD research network (www.polandaod.pl, accessed on 24 November 2021) is a consortium of Polish stakeholders established in 2011, focused on investigations of aerosol–climate interaction. The primary goal of the network is to conduct measurements of aerosol optical and microphysical properties (e.g., AOD, aerosol scattering and absorption coefficient, single scattering albedo, extinction vertical profile, and particle size distribution) and radiation surface budget components. In addition, radiative transfer and aerosol transport model simulations over Poland are used to quantify the aerosol–climate impact.

The main research objectives of the Poland-AOD network are the following:

- experimental studies and modelling of direct aerosol effect (at ground level and the top of the atmosphere),
- improvement of knowledge about long-term trends in aerosol optical properties and aerosol radiative forcing,
- understanding of the transformation of aerosol optical properties over Poland and the impact of urban emissions on columnar and surface aerosol optical properties,
- validation of indirect retrievals to determine AOD and SSA using satellite data and ground-based measurements,
- validation of aerosol transport models (e.g., GEM-AQ, WRF-Chem, NAAPS)
- developing new methodologies for observation and modelling of aerosol properties, including in situ and remote sensing technologies.

A crucial objective of the Poland-AOD network is to consolidate the national aerosol society on the country level. A national conference titled "The role of aerosol in climate processes" is organized every other year. In addition, winter and summer schools for bachelor, master, and doctoral students are conducted. These activities usually coincide with field campaigns, which allow students and young researchers to get involved in the Poland-AOD research program.

3. Research Stations

In 2021, the Poland-AOD network comprises 10 stations (Figures 1 and 2; Table 1): the Radiative Transfer Laboratory (RTlab) and the Remote Sensing Laboratory (RSlab) at the Institute of Geophysics, Faculty of Physics, University of Warsaw (FUW) in Warsaw (urban station); the research station of the Institute of Oceanology, Polish Academy of Sciences in Sopot (coastal-urban station); the Central Geophysical Observatory in Belsk (rural station) and the Silesian Geophysical Observatory in Raciborz (urban station) of the Institute of Geophysics Polish Academy of Sciences; the Meteorological Observatory

at the Nicolaus Copernicus University in Torun (urban station); the research stations in Rzecin and Debrzyna of the Poznan University of Life Sciences (both rural stations); the research station in Borucino of the University of Gdansk (rural site); the observational station in Wroclaw of the University of Wroclaw (urban site); and the private Radiative Transfer Station SolarAOT in Strzyzow co-operated by the FUW (background mountain station). For a more detailed description of the research, stations see Section S1 in the Supplementary Materials.

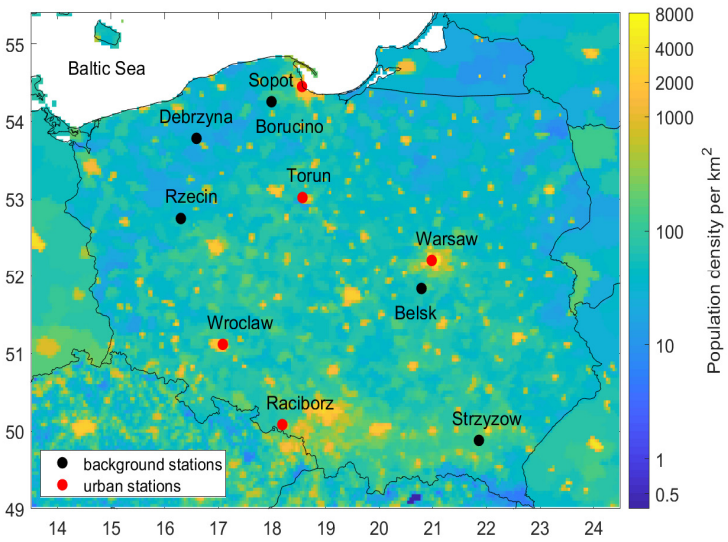

Figure 1. Locations of Poland-AOD aerosol research network stations. Red dots correspond to urban and black dots to rural (background) sites. The colour map shows population density in [km^{-2}] obtained from the Gridded Population of the World Version 4 of the Center for International Earth Science Information Network (CIESIN, https://sedac.ciesin.columbia.edu/data/collection/gpw-v4, accessed on 24 November 2021).

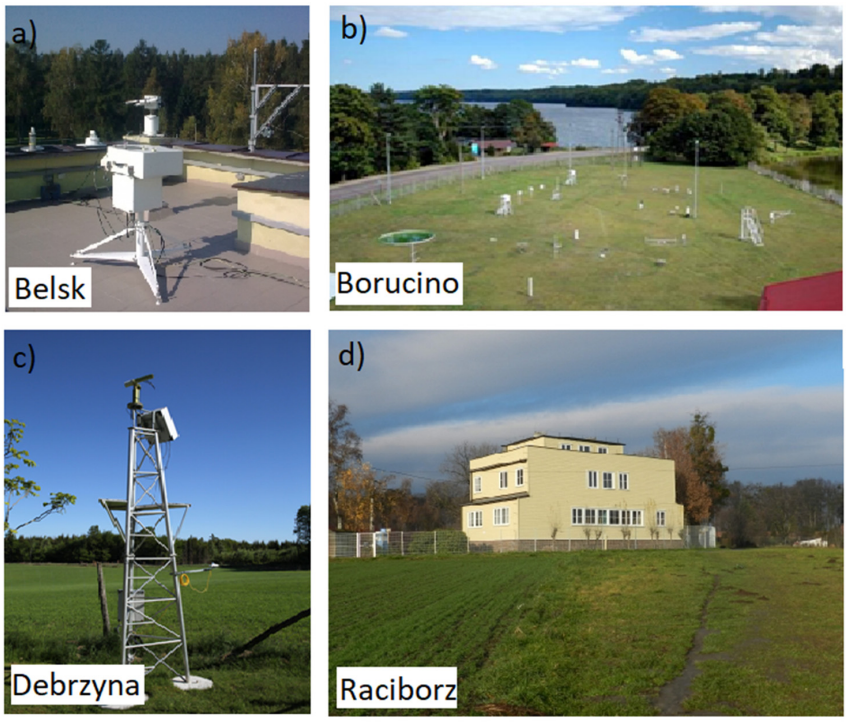

Figure 2. *Cont.*

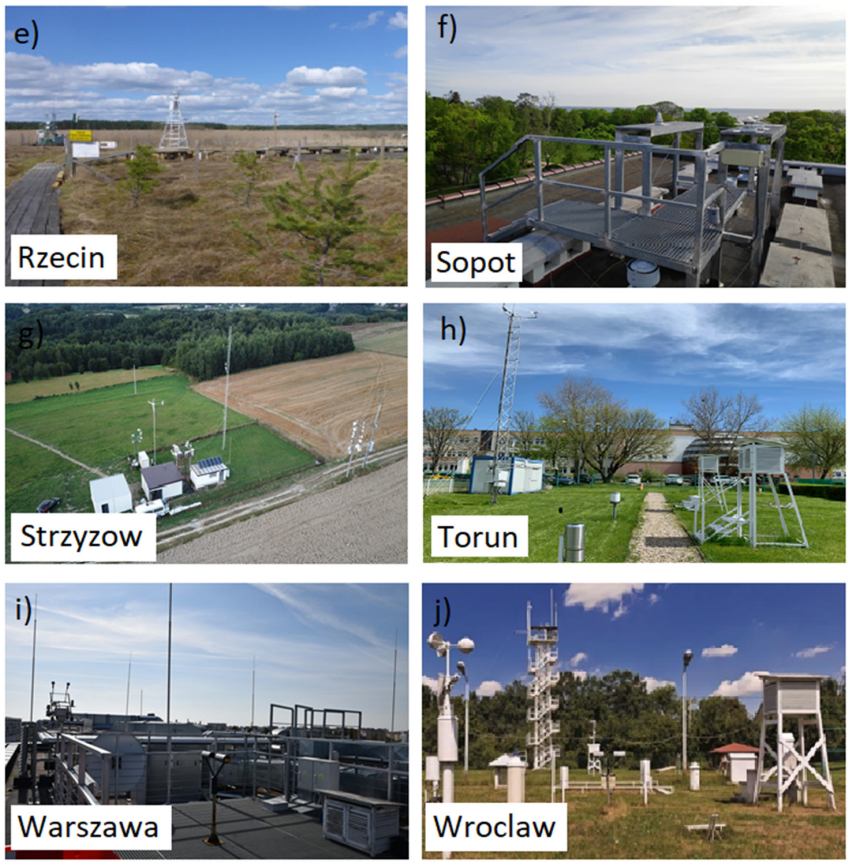

Figure 2. Poland-AOD research sites: (**a**) Belsk, (**b**) Borucino, (**c**) Debrzyna, (**d**) Raciborz, (**e**) Rzecin, (**f**) Sopot, (**g**) Strzyzow, (**h**) Torun, (**i**) Warsaw—roof platform, and (**j**) Wroclaw.

Table 1. Basic information about the Poland-AOD aerosol research network stations.

Station	Coordinates Lat., Lon., Alt.	Type of Station	Additional Information	Year Established
Belsk (IG PAS)	51.83 N, 20.80E, 180 m	Rural	EARLINET (2000) AERONET (2002)	1965
Borucino (UG)	54.26 N, 17.97 E, 163 m	Rural	-	1961
Debrzyna (PULS)	53.78 N, 16.59 E, 158 m	Rural	AERONET (2020)	2020
Raciborz (IG PAS)	50.08 N, 18.19 E, 230 m	Urban	AERONET (2015)	2015
Rzecin (PULS)	52.75 N, 16.31 E, 57 m	Rural	AERONET (2016)	2016
Sopot (IO PAS)	54.45 N, 18.56 E, 10 m	Costal-Urban	-	2011
Strzyzow (SolarAOT, FUW)	49.88 N, 21.86 E, 444 m	Rural-Mount	AERONET (2013)	2004
Torun	53.02 N, 18.57 E, 58 m	Urban	-	2009
Warsaw (FUW)	52.21 N, 20.98 E, 115 m	Urban	PollyNET (2013) EARLINET (2015) AERONET (2018)	2005
Wroclaw (UWr)	51.10 N, 17.09 E, 116 m	Urban	-	1946

4. Calibration

Data quality assurance involves the proper calibration of the equipment (Table 1). The calibration of sun photometers is performed at least once per year. The CIMEL is calibrated within the ACTRIS/AERONET network framework, while Microtops and MFR-7 are calibrated based on the Langley technique [19] within the Poland-AOD network. Microtops are calibrated at mountain sites (typically at SolarAOT in Poland), or at high mountain observatories such as Izaña in Tenerife, Zugspitze in Germany, and Kasprowy

Wierch in Poland. In addition, the Microtops are also calibrated against CIMEL sun photometers at different Poland-AOD stations (e.g., Warsaw, Strzyzow, Poland).

Radiometers are calibrated usually every 2–3 years by Kipp & Zonen. Pyranometers are intercalibrated within the Poland-AOD every 3–5 years. The zero-offset correction [20] for pyranometers, an effect of thermal radiation, rapid changes in ambient temperature, and heat dissipation by electronics, are estimated every night and applied to daily data of SW flux. This is minimized by using ventilation systems [21], which are used for most Poland-AOD sites.

Nephelometers are usually calibrated every 3–4 months with CO_2 gas, while photoacoustic extinctiometers are calibrated by the manufacturer (Droplet Measurement Technologies). The calibration of zero offsets for each nephelometer is performed every 24 h in the case of Aurora and every 10 min for the TSI nephelometer and PAX.

The low-cost aerosol particle counters are calibrated against Aurora 4000 nephelometer according to the methodology described in [22].

5. Data Processing

The data collected within the framework of the Poland-AOD network are available at three levels (1.0, 1.5, and 2.0). Level 1.0 includes raw data directly obtained from the instruments with different formats, which depend on software used for data acquisition. In general, these data are available in the ASCI or NetCDF format. Level 1.5 includes data with an initial calibration applied and after removing cloud contamination (in the case of sun photometers or clear-sky radiation). Level 2.0 contains the final calibration values applied to the data set. Data for Levels 1.5 and 2.0 are available in the MatLAB native format; however, data can also be exported to NetCDF files.

Data collection within Poland-AOD depends on measurement systems and ports to communicate between PCs and devices. For many instruments and RS232/RS485 ports, the software is written in Perl under the Linux system. It allows automatic control of the instruments and sending messages if an error with communication or any problem appears. Output from such software is a simple ASCII file. The Perl scripts are used for the following instruments: radiometer, MFR-7, weather station, nephelometers, aethalometers, and PAXs. In other cases, the original software is used, and automatic control is usually not possible. However, Linux scripts check if data from such instruments are saved in proper form and format.

Data processing is implemented at the Linux server at FUW. The Bash scripts are responsible for data transfer (e.g., receiving data from Poland-AOD stations and sending data to the www server), while MatLAB scripts are used for data processing. The automatic data processing starts every 1 h and includes data transfer from levels 1.0, 1.5, and 2.0. Processing of data for each instrument includes a module reading the native format and identifying the bad data, the script applying the calibration, correcting (both depend on specific measurement techniques), averaging and filtering. A module saving the data at levels 1.5 and 2.0. In addition, "quick looks" for any data are prepared for level 1.5. These figures (in png format) are available on the Poland-AOD website. Data processing for each instrument used the methodology described by the scientific literature.

Cloud screening is a critical process during the post-processing of data from a sun photometer [23] and a radiometer. In the first case, the cloud must be removed if it interacts with direct solar radiation. It is necessary to remove data if any cloud in the sky appears for radiometer, almucantar, and principal scans of diffuse radiation measured by sun photometer. Filtering cloud-contaminated AOD data obtained from MFR-7 measurements are based on automatic cloud-screening algorithms described in [24]. These are based on the temporal variability of the measured AOD. For solar flux radiation, the cloud mask algorithm is based on simple RTM [25]. The total solar flux simulated by this model is used to match the observation data. The minimization is performed with respect to AOD at 500 nm. Other input parameters such as AE, total water vapour, and SSA are taken from AERONET retrieval or climatology if instant data are not available. Next,

the measurements are assumed to be clear-sky if the difference between the model (with optimal optical parameters) and observation is smaller than 30 W/m^2 or 20 W/m^2 if solar flux is above 200 W/m^2 or below 200 W/m^2, respectively. The second criterion must be satisfied if the difference in standard deviation between model and observation is less than 0.8 W/m^2. The standard deviation is computed for the nearest nine points. This method allows the removal of both small convective as well as cirrus cloud data. In addition, the cloud contamination on incoming solar radiation is monitored by whole-sky cameras. The cloud fraction is computed based on an algorithm utilizing the R/B (red to blue) threshold. For cloudy pixels, the R/B ratio is flat; therefore, clear-sky pixels are defined when the R/B is higher than the assumed threshold. However, this threshold depends on the aerosol optical properties and zenith and azimuth angle. For this purpose, the single-scattering approximation RTM is used to compute the R/B for each image pixel. Input to this model is taken from AOD observation.

Processing the aethalometer and nephelometer data required several corrections. In the case of the nephelometers, the effect of light anisotropy (non-Lambertian illumination) and truncation of scattering angle must be considered. Such corrections for both TSI and Ekotech nephelometers are described in [26]. For the Aurora 4000, a slightly different method for truncation error is used. For this purpose, the method published in [27] was modified by estimating the correction factor based on the AE and the ratio of backscattering to the total scattering coefficient.

Data obtained from the aethalometer were according to the methodology proposed in [28]. In this filter-based aerosol measurement technique two effects must be accounted for. The multiple scattering correction is an effect of light scattering between the quartz filter fibres and aerosol embedded in the filter. This effect enhances the light absorption and leads to an overestimation of the aerosol absorption coefficient. The second correction, called the filter loading effect, can be explained by the increase in the attenuation of the signal by light-absorbing particles accumulating in the filter. Therefore, the optical path is reduced in a loaded filter, and the optical system is less sensitive to absorbing particles collected in a dirty filter. Both effects are corrected by the methodology described in [28]. This method utilized data on aerosol scattering, which are obtained from nephelometer observations.

Information on the PollyXT lidar data retrieval methodology is given in several papers, which are shortly described below. The approach used to evaluate the aerosol particles' optical property profiles is detailed in [16,29,30]. The raw lidar signals are evaluated according to the EARLINET/ACTRIS database quality assurance and quality checks (QA & QC) procedures. Data collected from 2013–2019 were evaluated manually. Since 2020, the data have been calculated only with SCC (single calculus chain) EARLINET/ACTRIS online evaluation software and every profile stored in the EARLINET/ACTRIS database. For the Warsaw lidar station, profiles were retrieved using the classical Raman approach as detailed in [29], i.e., the aerosol extinction coefficient (σ) profiles were evaluated with an assumption on extinction Ångstrom exponent (EAE). With known σ, the backscattering coefficient profiles (β) can be evaluated with an estimate of the β reference value at the reference height. The retrieval of all profiles using only the Raman approach makes the data set from the Warsaw lidar station unique. It allows, e.g., to calculate the lidar ratio profiles (LR = σ/β) and EAE profiles (obtained from σ at 355 and 532 nm) that are close to reality. The linear depolarization profiles (LDR) were obtained using the depolarization calibration constants calculated twice a day from automatized $\pm 45^\circ$ calibration measurements for each wavelength as detailed in [31,32]. To derive the particle optical properties, we used the radiosonde atmospheric profiles of the WMO 12,374 station in Legionowo (52.40° N, 20.96° E, located about 30 km from Warsaw lidar) data accessible via the University of Wyoming website (http://weather.uwyo.edu/upperair/sounding.html, accessed on 24 November 2021).

For the manual evaluation, the temporal averaging of the aerosol particle optical property profile is set either to 30, 45, or 60 min (depending on the day/night conditions, signal-to-noise ratio, and temporal cloud screening). The spatial resolution of profiles

is set to an initial 7.5 m and then smoothed with the running mean for 49 range-bins corresponding to 367.5 m (low-smoothing b-files) and for 101 range-bins 757.5 m (high-smoothing e-files). The temporal and spatial resolutions for the SCC evaluation are different for each property profile, being reduced/increased and smoothed according to the signal-to-noise ratio minimum requirement.

The retrieval of aerosol microphysical properties applied for the PollyXT lidar data is based on the availability of the 3β and 2σ profiles. It is calculated within layers of high values and low uncertainties. The derivation of the aerosol size distribution in the range of 30–1500 nm is possible with the complex refractive index constraints. Also, the particle concentration and the single scattering albedo can be provided. Different codes are used, e.g., the code of [33] is used as described, e.g., in [34], or the code of [35] is used as described in [36].

The approach for deriving the water vapour mixing ratio and the relative humidity profiles from the PollyXT lidar data are detailed in [37], whereby, for the calibration of the latter data product, the radiosonde profiles in Legionowo are used. The water vapour profiles are derived typically with higher temporal and spatial averaging than the aerosol particle optical properties.

The use of the lidar data for deriving the ABLH with the wavelet transform is detailed in [38] and with the gradient and saddle point method in [39]. The methodology for the retrieval of the AOD within the boundary layer (AOD_{BL}) and the entire troposphere using an iterative extrapolation (lower range) and interpolation (upper range) from the lidar data are detailed in [16,17]. The aerosol typing schemes applied for the lidar data for the case of the molecular aerosol and cloud scattering separation are described in [38] and for fine/coarse mode dust and anthropogenic pollution in [40].

6. Integration of Aerosol Measurements with ATM

The radiation fluxes, instantaneous direct ARF, and profile of radiation heating rate in the lower atmosphere are computed by the RTMs. For this purpose, the interfaces between the Poland-AOD database and Moderate-Resolution Atmospheric Radiance and Transmittance model (MODTRAN) ver. 5.3 [41] and Fu-Liou ver. 200412 [42] codes were developed (Figure 3). Direct ARF is defined as the difference between the net (downward minus upward) SW radiative fluxes representing atmospheres with and without aerosol load under clear-sky (cloud-free) conditions

$$\mathbf{ARF} = (\mathbf{F}\downarrow - \mathbf{F}\uparrow)_{\mathbf{polluted}} - (\mathbf{F}\downarrow - \mathbf{F}\uparrow)_{\mathbf{pristine}} \quad (1)$$

where the first parenthesis describes aerosol-perturbed net SW flux, while the second parenthesis describes the same quantities but for the aerosol-free case. The clear-sky ARF is computed based on two methods. The first (the so-called hybrid method) uses the surface observation of SW fluxes (for aerosol case) and RTM simulation of aerosol-free radiation fluxes [43]. In the second approach (the so-called model method), both polluted and pristine conditions are simulated by the RTM. The first method can be used to estimate the surface ARF only. In the case of the second method, the ARF at the top of the atmosphere (tropopause and in the atmosphere) can be calculated. The RTMs are configured to run simulations automatically for each Poland-AOD station.

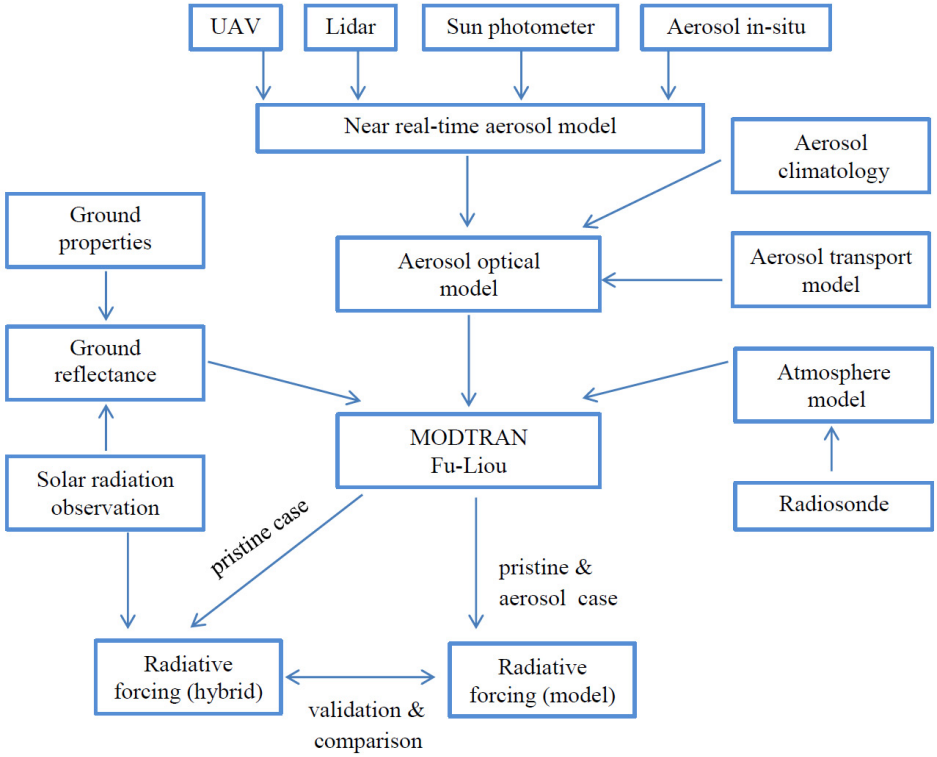

Figure 3. Diagram of the RTM interface with the Poland-AOD database.

The input to both RTMs contains several modules with different options depending on available data. For the thermodynamic parameters, the radiosonde profiles or standard profiles can be applied. They can be profiles obtained during Poland-AOD activity (field campaign), profiles downloaded automatically for appropriate (the closest) WMO stations, or data from climatology. In the second and third cases, the water vapour profile is scaled to the total water vapour content measured by sun photometers. The surface module includes information about spectral ground reflectance. For this purpose, the climatology of surface reflectance is defined based on the AVHRR observation (CLARA-2) product [44]. Broadband albedo measurements can be used to scale spectral reflectance.

Aerosol optical properties are defined in the near-real-time aerosol module. This segment is connected with results of lidar and UAV soundings and columnar parameters from sun photometer measurements and surface in situ observations. Also, the climatology information and aerosol transport model simulation results can be used if some observations are not available (e.g., extinction profiles, SSA). The aerosol input includes the following information: spectral AOD, SSA, asymmetry parameter, and profile of aerosol extinction coefficient at 550 nm. The SSA can be applied as a columnar value based on AERONET indirect retrieval (level 1.5 or 2.0) or from surface in situ observation (assuming surface value as a columnar), and also as a vertical profile based on the aerosol transport model or the UAV observation (see [45] for the methodology). The asymmetry parameter can be set as a columnar value only, that because the profile of this parameter is not currently measured. In the case of the aerosol extinction profile, data from lidar or ceilometer retrieval (elastic or Raman channel) can be used as well as an exponential profile with the surface value measured by both nephelometer and aethalometer. The sensitivity study of ARF due to different aerosol parameterization for MODTRAN and Fu-Liou models was discussed in [46].

7. Field Campaign Activity

The activities of the Poland-AOD network are not limited to continuous and quasi-continuous observations at research stations but also expand to intensive field experiments. During the last decade, several joint field campaigns have focused on different aspects of

aerosol and aerosol–climate research in Poland. The experiment in Rozewie, Baltic coast in 2009 focused on studies of aerosol vertical structure and AOD in the coastal areas [47]. This work shows that the contribution of fine and coarse mode particles in AOD depends on the direction of air mass advection (long-range and sea-land breeze). During the COastal Aerosol STudies (COAST) campaign (28 July–3 August 2011), simultaneous aerosol optical depth measurements were conducted at four locations in the Baltic Sea region, i.e., Sopot (Poland), Preila (Lithuania), Liepaja (Latvia), and on the island of Bornholm. Aerosol optical depth measurements obtained with Microtops II sun photometers were used to validate the MODIS retrieval close to coastal regions. The satellite and sun photometer measurements agreed well. The mean bias and RMS of the AOD at 500 nm were less than 0.005 and 0.03, respectively [48].

The campaign in September 2010 in Strzyzow, was focused on the direct aerosol effect while also testing and calibrating different devices to measure aerosol optical properties. In particular, a new satellite algorithm developed at FUW for the AOD retrieval from SEVIRI observations was validated [49]. The HyMountEcos (Hyperspectral Remote Sensing for Mountain Ecosystems) campaign in Karpacz (mountain region in south-western Poland) in June and July 2012 [50] was focused on the determination of atmospheric correction of satellite land imaging. For this purpose, a combination of the lidar and sun photometric observations was used, and particle vertical profiles from aerosol transport models. A comparison of the results from models shows reasonably good agreement with observations of aerosol vertical distributions and their temporal variability during a Sahara dust event in July 2012 [51].

A campaign in Slupsk (October 2015) investigated the relationship between sea spray fluxes and underwater whitecap noise [52]. The dependence of underwater sound pressure level on sea-spray fluxes was found, and it was explained by physical differences in wind wave development and its relationship with wave age or mean wave slope. During a coastal campaign in Władysławowo, Poland (January and February 2015), aerosol transformation in the atmospheric boundary layer above the Baltic Sea was investigated [53] using multi-wavelength lidar. A retrieval algorithm for aerosol size distribution from multiwavelength lidar profile observations was developed. It was found that under strong wind conditions from the open sea, aerosol particle effective radii were larger and decreased monotonically with altitude, which was attributed to the emissions of coarse aerosol particles from the sea surface covered by spume. The observations suggest a need to verify the present aerosol generation functions and sea-spray distribution parameterization implemented in weather models.

The first tests of aerosol profiling with miniaturized equipment installed on the UAV and tethered balloons were performed during summer campaigns in Strzyzow in 2013, 2014, and 2015 and the winter campaigns in Swider (about 20 km from Warsaw) in 2014 and 2015. AE-51 aethalometers, OPC-N2 particle counters, and RS92SGP radiosondes (as a set of weather sensors) were mounted on fixed-wing and hexacopter UAVs to profile the low troposphere (up to about 1 km a.g.l.). In addition, the ground-based LB-10 lidar (Strzyzow), CHM15K ceilometer (Strzyzow), and CL31 ceilometer (Swider) observations were used to compare remote sensing data with in situ information obtained from miniaturized devices. The profiles of eBC mass concentration show multi-layer structures similarly to the lidar/ceilometer signals [54]. During winter UAV flights, it was discovered that the intensive smog layer (eBC up to 40–60 $\mu g/m^3$) could be very shallow (up to 50–100 m a.g.l.), below the ceilometer minimal altitude of detection [55].

Measurement campaigns in mountain regions in southern Poland in Krynica Zdroj (March 2016) and Bielsko-Biala (February and March 2018 and 2019) focused on developing a methodology to measure the vertical structure of absorbing aerosols in the mountain regions. For this purpose, miniaturized equipment such as the AE-51 aethalometer, OPC-N2 and PMS7003 particle counters, and weather sensors were mounted on the cable cars to Jaworzyna Krynicka (1114 m a.s.l.) and Szyndzielnia (1028 m a.s.l.), respectively. In both cases, the FUW mobile laboratory, with aerosol microphysical and optical properties

devices situated at the bottom of the valley, was used to identify aerosol single-scattering properties. Results from Krynica Zdroj [56] show a significant correlation between the air temperature gradient and the difference in extinction and scattering coefficients between the valley and mountain top. In addition, data obtained from OPC-N2 indicates a significant vertical variability of fog and smog microphysical parameters. Results from an experiment in Bielsko-Biala indicate a high reduction in aerosol mass concentration (total and eBC) with altitude only in the morning hours [57]. In addition, observed changes in the vertical structure of the aerosol mass concentration in the 30 min interval can be explained by the mixing processes (mountain–valley breeze circulation). Observations at Bielsko-Biala indicate that surface air inversion is the main factor influencing the level of extensive aerosol optical and microphysical properties [57].

Two summer POLIMOS (Polish Radar and Lidar Mobile Observation System) field campaigns in 2018 and 2019 took place at the Rzecin and Warsaw stations. Both campaigns focused on a characterization of the atmospheric composition obtained from different combinations of remote sensing and in situ instrumentation, such as the ESA Mobile Raman Lidar EMORAL, the PollyXT lidar, the BASTA 95GHz Doppler cloud radar (provided by LATMOS, France), the HALO Doppler lidar (provided by the University of Granada, Spain), the HATPRO microwave radiometer (provide by INOE, Romania), the CIMEL photometer, the static chamber sites for CO_2, CH_4, and water vapour flux measurements. The synergy of data obtained from remote sensing instruments was used to discriminate molecular, aerosol, and cloud particles [30], to assess the contribution of free troposphere aerosols to total aerosol loading within the troposphere [40,58] and stratosphere [59], including ongoing work on estimation of the aerosol vertical fluxes within the boundary layer.

8. A Brief Overview of Poland-AOD Network Results

The network research focused on several aerosol–climate aspects. The most important finding of the aerosol–climate effect was the indication that systematic reduction in aerosol loading observed during the last 3–4 decades over Poland reduces negative ARF. The mean AOD trend is −0.06 per decade and AOD exhibited a reduction of about 50% between 1982 and 2015 [60]. However, the influence of aerosol loading reduction on the radiation budget was significantly higher in the last decade of the 20th century compared to the first decades of the 21st. The positive trend of ARF is significantly higher than the trend of greenhouse gases RF [60]. The effect of aerosol reduction explains the enhancement of climate warming observed in the last decades, especially during the summer season.

On the other hand, the impact of aerosol on winter warming is significantly smaller due to low solar radiation flux and lower AOD and higher cloud cover than in summer. Reduction in AOD in the last decades (since 1964) is estimated from long-term direct observation of broadband and wideband solar flux at Belsk [61] and WMO stations in Zakopane [62] and Kasprowy Wierch [62,63]. For this purpose, a methodology to retrieve broadband and wideband AOD is being developed [63] within the Poland-AOD network. The results of this study show a significantly lower reduction in AOD obtained for the high mountain station (Kasprowy Wierch) in comparison to the Belsk and Zakopane sites, but also the opposite annual cycle of AOD at Mount Kaprowy Wierch to the AOD defined in the vertical column (1140 m) from Zakopane valley to Kasprowy Wierch, which is similar to the PM_{10} concentration measurements in Zakopane [62]. Both can be explained by reducing anthropogenic emissions rather than natural emissions variability (e.g., volcanic).

Several studies have focused on describing the aerosol long-range transport in light of particle optical and microphysical properties and their effect on the radiation budget. Such events are observed mostly during spring and summer when natural aerosol emissions are at their maximum, and deep convection transports air pollution to the middle and the upper troposphere. In recent years, lidar observations have shown high biomass burning activity from wildfire emissions in Europe (mostly from Ukraine) and North America [15,16,34,36,59]. The transport of biomass burning from Ukraine, as detailed in [16], indicates the intrusion of smoke particles into the urban, planetary boundary layer.

This process is identified by an increase in AOD and AE and surface PM_{10} and $PM_{2.5}$ mass concentration and an increase in the PBL top height. Transport of biomass burning particles was identified between the lower and upper troposphere and occasionally in the lower stratosphere [59]. The optical properties of the biomass burning particles showed moderate absorption due to the oxidation process and water uptake during several days of transport from the source region. It was found that moderate absorbing particles (mostly from biomass burning) significantly impact sensible and latent heat flux at the surface [46].

The methodology of integrating data obtained from UAV, tethered balloon, and cable car profiling with lidar observations was developed [55,64]. This method allows the SSA profile to be obtained and extends the lidar signal below the overlap latitude. Vertical profiling of the surface aerosol layers by moving platforms is important during the winter and intensive smog conditions. This information can be utilized by models to improve air quality forecasts. Moreover, a new scheme for determining molecules, aerosol (spherical, non-spherical, fine, coarse), cloud phase (liquid, ice, supercooled droplets), and precipitation (drizzle, rain) from combined data obtained from the Raman lidar, cloud radar, and microwave radiometer at the Rzecin site was developed in [30]. The optical properties of the atmosphere and CO_2 exchange data collected at this site in 2018 were also used to quantitatively estimate atmospheric optics' impact on peatland productivity. It was found that the increase in AOD values could determine the CO_2 uptake increase in this ecosystem under cloud-free conditions [65].

The research focused on the relation between columnar data and surface optical properties or $PM_{10}/PM_{2.5}$ revealed specific characteristics. Data for short periods, especially from the summer, showed moderate and relatively high correlation coefficients between AOD and the scattering coefficient or $PM_{10}/PM_{2.5}$ [66]. In contrast, the correlation coefficient was negative for a longer period, which was a consequence of a different annual cycle of AOD and PM_{10} ($PM_{2.5}$) [67]. The cold season emissions by the heating system showed a significant effect on air quality (PM_{10}, $PM_{2.5}$) only in the first hundreds of metres, which weakly affect columnar AOD. The peaks of AOD are observed in spring and summer when the PM_{10} ($PM_{2.5}$) was low. This can be explained by the variability of PBL height and convective transport of aerosol to the upper levels during the warm season [68]. The summer PBL height is two to three times higher than the winter value [38,39,69]. Variability of AOD with PBL height was confirmed by lidar and sun photometer observations over Warsaw [58].

An extension to land studies within the PolandAOD network comprises measurements made on board the research vessel s/y Oceania of the Institute of Oceanology Polish Academy of Sciences during cruises to the Baltic Sea. The ship-borne studies are focused on air–sea interaction phenomena and optical properties of the aerosol particles. The cruise measurements result in a large database of the in situ sea-spray (coarse mode) aerosol concentrations and fluxes. Since 2011, 224 h of sea-spray fluxes have been obtained using the gradient method [70]. The flux measurements were used to determine the very first sea-spray generation function for the Baltic Sea [71]. The sea-spray generation function varies regionally; therefore, a separate function for the Baltic Sea is important to improve the quality of regional atmospheric and air-sea interaction models.

Sea-spray fluxes over the Baltic Sea depend on wave properties. Preliminary studies [72] have indicated that two major regimes of wave conditions (developing and developed waves) are characterized by two different flux magnitudes (an order of magnitude higher in number emissions for developing waves). Furthermore, when compared with our measurements, two generation functions given in [73] showed the influence of wave age and the physical properties of the wave field on sea-spray emissions. Sea-spray fluxes can be obtained using the gradient method and eddy covariance method [74,75]. The application of both methods to our cruise dataset and comparison of the results are presented in [76]. The scaling method of gradient aerosol fluxes (indirect method) by eddy covariance (direct) is also presented. This new approach can be used in any other geophysical experi-

ment to compare different methods of measurements. This will allow, e.g., the turbulence diffusion coefficient for sea spray to be determined in future studies.

Modelling research focused on validating the AOD product in GEM-AQ [77,78] during long-range transport events. Preliminary model calculations aimed to reproduce the AOD over Poland for the transport of the biomass burning smoke episode in the period 30 April–4 May 2012. The model was able to capture the average AOD before the episode and the observed increase in AOD at ground-based stations. However, the peak values were overestimated (mainly in the mid troposphere). After launching the operational forecast, the comparison undertaken from mid-March to mid-September 2016 showed that the AOD forecast was overestimated. The variability of forecasted AOD had a significantly lower amplitude than observations. The spatial pattern of AOD calculated as a six-month average for the same period was dominated by mineral dust aerosol. This led to the revision of the on-line dust uptake parameterization.

Further analysis from March 2016 to March 2017 showed that the modelled spatial distribution of AOD was highest during the spring months (0.25–0.4), which was due to an episode of Saharan dust transport (4–7 April). During the summer period, the monthly average AOD varied from 0.35 in June to 0.25 in August. In the autumn, the AOD gradually decreased from 0.2 in September to 0.1 in November. The lowest values were forecasted for the winter period (0.1–0.15). Further evaluation analysis of forecasted AOD vs. observation showed good performance in the timing of long-range transport events of Saharan dust or biomass burning. At the same time, the background variability indicated the importance of aerosol distribution in the mid troposphere, which is problematic in terms of observational data.

There is ongoing work on implementing air quality and satellite data assimilation in the WRF-Chem model [79]. The preliminary results show a significant difference in the impact of surface ($PM_{2.5}$ concentrations) and satellite (AOD) data assimilation on the modelled particulate matter concentrations between the summer and winter periods, which to a large degree is related to the availability of satellite data. The study suggests that severe winter air pollution episodes in Poland and Eastern Europe, often related to the dense cover of low clouds, will benefit from the assimilation of surface observations rather than satellite data, which can be very sparse in such meteorological situations.

9. AOD and ARF Results

Clear-sky direct ARF at Poland-AOD sites between 2011 and 2019 was obtained from Fu-Liou RTM simulations. ARF is estimated based on a model method (see Section 8) utilizing aerosol optical properties from observation and Aerosol Analysis and Prediction System (NAAPS) reanalysis [80]. The NAAPS AOD agrees quite well with observations from Poland-AOD stations (see Figure S1 for more details). The mean AOD at 550 nm (Figure 4) changes from approximately 0.14 to 0.17. The smallest value was observed at the SolarAOT (mountain) station, while the highest was at Raciborz (Upper Silesian Industrial Region), and it was slightly lower in Warsaw and Belsk. Similar spatial distribution was obtained for surface and TOA ARF. The surface clear-sky ARF changes from -8.7 to -5.0 W/m^2, while TOA ARF from -5.0 to -4.3 W/m^2.

The mean AOD trend during the last years (2011–2019) is -0.02/10 yr (Figure 5a). Previous research [60] shows mean AOD trends of approximately -0.06/10 yr between 1982 and 2015. The reduction in the AOD negative trend observed during the last years can be explained by the relatively slow improvement of Poland's air quality compared to the rapid reduction in industrial emissions in the 1990s. The current transformation of residential heating systems from coal to greener fuels is continuing. Therefore, a reduction in AOD is expected in the future (especially in the cold season).

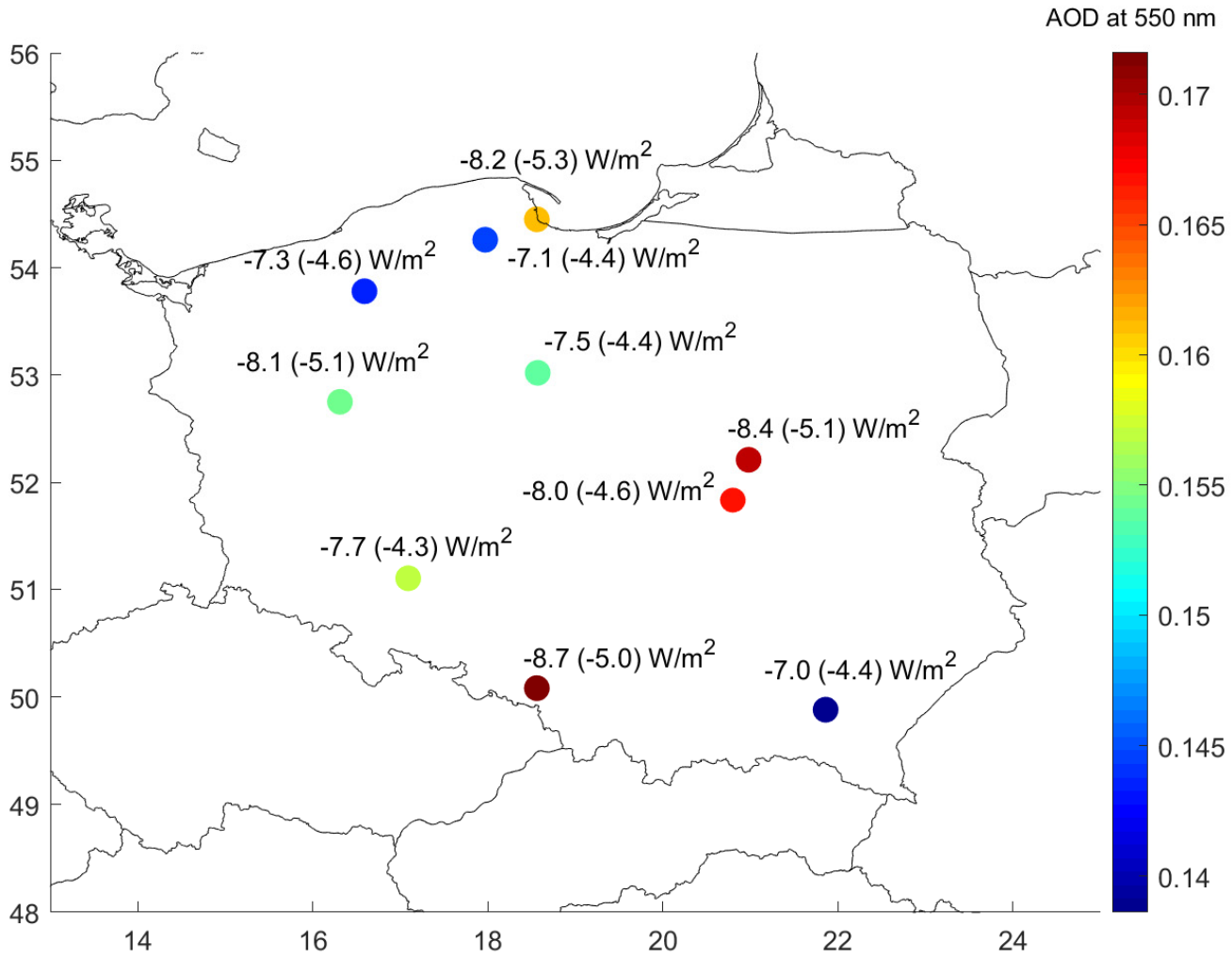

Figure 4. Spatial distribution of 2011–2019 mean AOD at 550 nm (colour scale) and surface and TOA (in parenthesis) ARF in W/m^2 at Poland-AOD stations.

A consequence of AOD changes is a reduction in TOA and surface ARF. The mean trend of clear-sky ARF is 0.34 $W/m^2/10$ yr and 0.68 $W/m^2/10$ yr at TOA and at the Earth's surface, respectively. In comparison, the mean ARF trend between 1982 and 2015 was 1.5 $W/m^2/10$ yr for TOA and 1.2 $W/m^2/10$ yr for the surface [60]. The positive trend of ARF contributes to climate warming, which is mainly forced by increased concentrations of greenhouse gases on a global scale. However, on a local scale, direct and indirect aerosol effects may significantly contribute to changes in the energy budget. The atmosphere ARF trend is negative (-0.35 $W/m^2/10$ yr), indicating a reduction in absorption of solar flux by aerosol particles. The consequence of that can be the enhancement of sensible and latent heat flux from the surface to the lower troposphere.

Annual cycles of AOD and ARF (Figure 6) show significant variability. The increase in AOD in spring and summer can be explained by the growth of natural emissions (mostly mineral dust and biomass burning transported from Europe and different continents) and intensive vertical transport of particles compared to winter [68]. Although maximum surface aerosol concentration (e.g., $PM_{2.5}$, PM_{10}) is observed during the cold season, the impact of the surface layer pollution (mostly from residential heating) on AOD is relatively small.

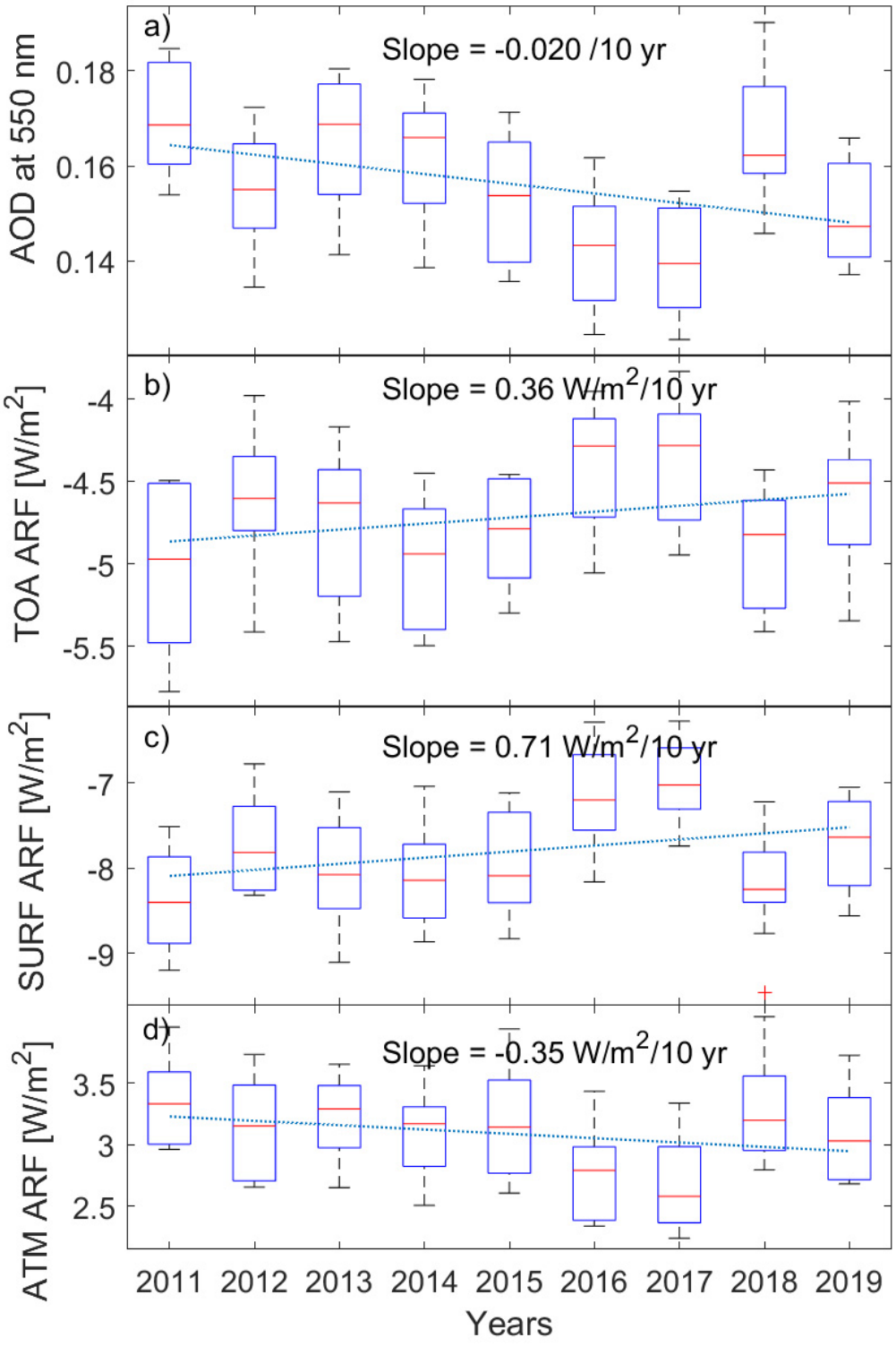

Figure 5. Box-whisker plots for annual mean AOD at 550 nm (**a**), clear-sky the TOA ARF (**b**), surface ARF (**c**), and atmosphere ARF (**d**) in [W/m^2] for Poland-AOD sites. The red horizontal lines show the median values. The lower and upper boxes correspond to lower (0.25) and upper (0.75) quantiles, while short horizontal lines show the lowest and highest values. The dotted lines show the linear fit.

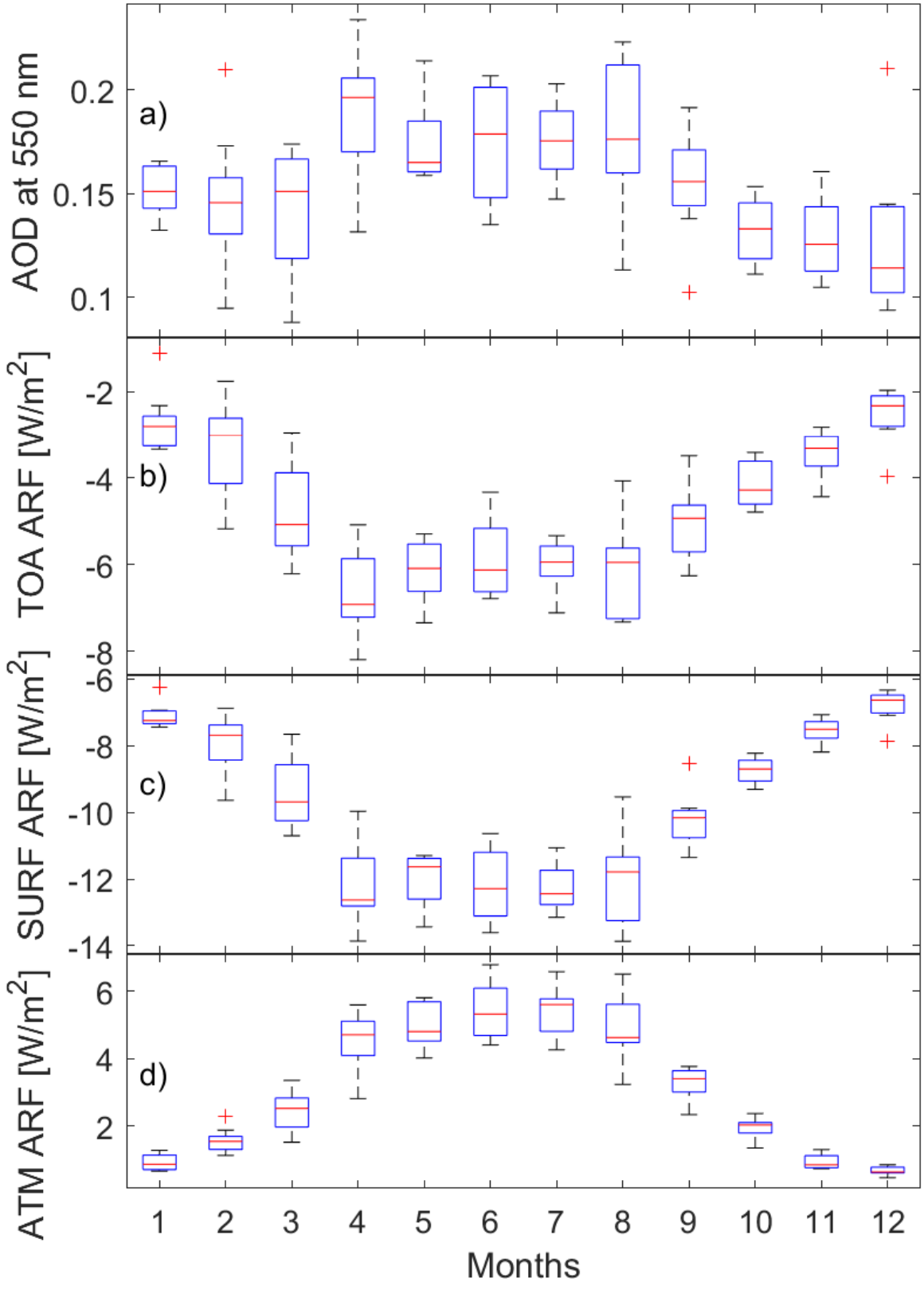

Figure 6. Box-whisker plots for the annual cycle of AOD at 550 nm (**a**), clear-sky TOA ARF (**b**), surface ARF (**c**), and atmosphere ARF (**d**) in [W/m^2] for Poland-AOD sites. The red horizontal lines show the median values. The lower and upper boxes correspond to lower (0.25) and upper (0.75) quantiles, while short horizontal lines show the lowest and highest values. The dotted line shows the linear fit.

The annual cycle of ARF is mainly a consequence of variability of incoming solar flux but also temporal changes of the aerosol optical properties. Therefore, significantly more negative ARF at TOA and the Earth's surface is observed during spring and summer than in winter. The TOA ARF changes from approximately -9 W/m^2 in April to -2 W/m^2 in December. The surface ARF varies from -12 W/m^2 (April, July) to -5 W/m^2 (December). The monthly ARF difference between winter and spring/summer is smaller than the variability of solar flux at TOA (approximately six times higher during summer than winter). It can be explained by the variability of radiation scattered to space with the solar zenith angle (ARF is associated with an upscatter fraction of solar energy). Due to the shape of the aerosol scattering phase function (which mainly decreases with the scattering angle), the upscatter flux at sunset and sunrise is greater than that at local noon. For example, for a solar zenith angle of 0° the scattering angle for upward radiation is 180°, while for a solar zenith angle of 90° the scattering angle is also 90°. The combination of two effects (decrease in solar flux and increase in upscatter fraction with the solar zenith angle) results in an ARF minimum (more negative) for solar zenith angles between 50° and 70° [81]. Therefore, during autumn and winter, the clear-sky ARF is still significant and not negligible. The ARF in the atmosphere is positive, with a maximum in July (5.5 W/m^2) and a minimum in December (0.7 W/m^2). This quantity describes the absorption of solar flux by particles suspended in the atmosphere.

10. Conclusions and Summary

Ten years of aerosol research within the Poland-AOD network has allowed the development of equipment infrastructure and data processing systems and improved knowledge on local aerosol–climate interaction. The network research has focused on several aerosol–climate aspects, e.g.,:

- Long-range transport of biomass burning and mineral dust;
- Air mass transformation;
- The effect of the megacity on aerosol optical properties;
- Relationships between columnar and surface optical properties;
- Temporal variability of the aerosol mixing layer;
- Long-term variability of aerosol properties and ARF;
- Integration of UAV, cable cars, lidar, and sun photometer observations;
- Aerosol-cloud typing.

The Poland-AOD research uses ground-based stations located in both rural (five sites) and urban (five sites) environments, supported by numerical model simulations (GEM-AQ, WRF-Chem), satellite observation, and different databases and re-analysis (e.g., CAMS, MERRA-2, NAAPS).

The main Poland-AOD network findings are:

- Improving the knowledge on the vertical structure of optical and microphysical aerosol properties, especially in the surface (smog) layer during the winter season.
- The surface smog layer usually has a depth ranging from several dozen to a few hundred metres and is poorly represented in aerosol transport models.
- Simulation of direct clear-sky ARF shows a continuation of positive trends at TOA and the Earth's surface because of AOD reduction (about 0.02 per decade). Less negative ARF contributes to climate warming by increasing the net solar flux at the surface and decreasing reflected solar radiation at the TOA.
- Smaller AOD trend at high mountain station (Kasprowy Wierch) can be explained by reduction in the anthropogenic emissions rather than natural emissions.
- Several case studies of aerosol long-range transport were used to define optical and microphysical particle properties (mainly biomass burning and mineral dust) as well their effect on the radiative budget and sensible and latent heat fluxes.
- During biomass burning events, the intrusion of particles into the urban boundary layer is observed and confirmed by the decrease in surface air quality.

- The fraction of the fine and coarse mode dust particles for long-range transported mineral dust and local agricultural dust is distinctly different.
- Intrusion of anthropogenic pollution via long range transport into urban boundary layer can result in enhancing boundary layer height.

Future research within the Poland-AOD will be focused on the following aspects:

- Continuation of integration of data from different instruments and platforms (including lidars, sun photometers, UAV, cable cars, satellite detectors);
- Extension (to the middle troposphere) of the vertical range of the UAV profiles, which until now has been limited to approximately 1 km, and automation of such measurements;
- Reduction in noise in low-cost sensors (especially under clean conditions) to improve sensor calibration and compensation of instrument artefacts due to UAV vibrations, airflow, and temporal variability of relative humidity in micro aethalometers (e.g., AE-51, AM-200);
- Data assimilation to aerosol transport models (GEM-AQ, WRF-Chem and EMEP4PL) including columnar and vertical profile data;
- Model validation and improvement of air quality forecast during low-level inversion conditions;
- Aerosol hygroscopicity covering in situ and remote sensing methods;
- Development of new instruments, especially a miniaturized sun photometer onboard the UAV to validate profiles of aerosol extinction and AE in the lower troposphere;
- Exploring synergies of different lidar types used for aerosol flux determination within boundary layer;
- Building the database for estimations of the impact of atmospheric optics on ecosystem functioning.

The scientific topics will be focused mostly on estimating contributions of local (national) emissions to the total AOD over Poland, on the transformation of columnar optical properties during transport of clean arctic air masses, on the vertical transport of aerosol from the free troposphere to the PBL and vice versa, but also the aerosol impact on the thermal structure of the PBL.

Intensive development of aerosol research infrastructure in Poland is expected during the next 1–3 years. This improvement will be performed with the ACTRIS-PL infrastructure development. In particular, new aerosol and wind lidars, cloud radars, and aerosol in situ devices will be installed at Poland-AOD stations.

Supplementary Materials: The following are available online at https://www.mdpi.com/article/10.3390/atmos12121583/s1. Figure S1: Comparison of AOD at 550 nm obtained from Poland-AOD observation with results of numerical simu-lation from NAAPS reanalysis. Dotted lines show perfect agreement. Measurement data were matched to NAAPS 6 h AOD product with 1 h time window. Ther corresponds to Pearson correlation coefficient, RMSE is root mean square error difference, BIAS is mean bias, and Number corresponds to number of data. Table S1: Instruments used within the Poland-AOD network. Index N indicates instruments to be purchased in 2021–2023 within the ACTRIS-PL infrastructure development (allocated funds).

Author Contributions: Conceptualization, K.M.M., T.P., T.Z.; data curation, W.K., A.S., A.P., P.P., J.M.; methodology, K.M.M., I.S.S., D.W. and A.K.R.; funding acquisition, L.B.; software, M.T.C., I.S.S., D.N.; validation, M.T.C., I.S.S. and O.Z.-M.; writing—original draft, K.M.M., I.S.S., M.P., B.H.C., K.M.H., J.S., J.W.K., M.W., M.K., M.M., P.M. (Przemyslaw Makuch), P.M. (Piotr Markuszewski), J.U.-K., K.W., A.D.-O., T.S. and A.R.; writing—review and editing, I.S.S.; visualization, K.M.M. All authors have read and agreed to the published version of the manuscript.

Funding: Equipment at Poland-AOD stations was obtained with the following grants of the National Science Centre in Poland: 2012/05/E/ST10/01578 (FUW), 1283/B/P01/2010/38 (FUW), 1276/B/P01/2010/38 (FUW), 2016/23/D/ST10/03079 (IG PAS), UMO-2017/27/B/ST10/00549 (FUW), UMO-2016/23/B/ST10/01797 (UWr), UMO-2017/25/B/ST10/00926 (UWr), UMO-2017/25/B/ST10/01041 (UWr), 2020/38/L/ST10/00480 (FUW), UMO-2017/27/B/ST10/02228 (PULS), UMO-2017/25/B/ST10/01650 (IG PAS) grant of Polish Foundation of Science and Technology:

519/FNiTP/115/2010 (FUW) grant of National Centre for Research and Development: Pol-Nor/196911/38/2013 (FUW, IO PAS), Investment Program of the Faculty of Physics of the University of Warsaw: 0801-D111-00110-01/MPK/1110300, and grants from European Union: POIG 01.01.02-22-011/09-00 (IO PAS) and structural funds POIR.04.02.00-00-D019/20-00 (UWr, FUW, IGF PAS, PULS).

Institutional Review Board Statement: Not applicable.

Informed Consent Statement: Not applicable.

Data Availability Statement: Poland-AOD data provided by the FUW are available to registered users or on request (https://polandaod.pl, accessed on 24 November 2021). The quick-looks are available at the Poland-AOD website (https://www.igf.fuw.edu.pl/~kmark/stacja/PolandAODdata.php, accessed on 24 November 2021). Access to archival data for different stations is provided through different portals (e.g., https://opendata.meteo.uni.wroc.pl for Wroclaw, accessed on 24 November 2021). The data products of CIMEL photometers observations at stations in Belsk, Debrzyna, Raciborz, Rzecin, Sopot, Strzyzow, and Warsaw are available via the AERONET portal (https://aeronet.gsfc.nasa.gov/, accessed on 24 November 2021). The data products of the lidar observations in Belsk in Warsaw are available via the ACTRIS Data Centre portal (https://actris.nilu.no/, accessed on 24 November 2021).

Acknowledgments: We are thankful to the technical staff for assisting in aerosol monitoring.

Conflicts of Interest: The authors declare no conflict of interest.

References

1. Myhre, G.; Myhre, C.E.L.; Samset, B.H.; Storelvmo, T. Aerosols and their Relation to Global Climate and Climate Sensitivity. *Nat. Educ. Knowl.* **2013**, *4*, 7.
2. Stocker, T.F.; Qin, D.; Plattner, G.-K.; Tignor, M.; Allen, S.K.; Boschung, J.; Nauels, A.; Xia, Y. *Climate Change 2013: The Physical Science Basis. Contribution of Working Group I to the Fifth Assessment Report of the Intergovernmental Panel on Climate Change*; Bex, V., Midgley, P.M., Eds.; Cambridge University Press: Cambridge, UK; New York, NY, USA, 2013; p. 1535. [CrossRef]
3. Aas, W.; Mortier, A.; Bowersox, V.; Cherian, R.; Faluvegi, G.; Fagerli, H.; Hand, J.; Klimont, Z.; Galy-Lacaux, C.; Lehmann, C.M.B.; et al. Global and regional trends of atmospheric sulfur. *Sci. Rep.* **2009**, *9*, 953. [CrossRef]
4. Bergin, M.S.; West, J.J.; Keating, T.J.; Russel, A.G. Regional atmospheric pollution and transboundary air quality management. *Annu. Rev. Environ. Resour.* **2005**, *30*, 1–37. [CrossRef]
5. Holben, B.N.; Eck, T.F.; Slutsker, I.; Tanré, D.; Buis, J.P.; Setzer, A.; Vermote, E.; Reagan, J.A.; Kaufman, Y.J.; Nakajima, T.; et al. AERONET—A federated instrument network and data archive for aerosol characterization. *Remote Sens. Environ.* **1998**, *66*, 1–16. [CrossRef]
6. Smirnov, A.; Holben, B.N.; Slutsker, I.; Giles, D.M.; McClain, C.R.; Eck, T.F.; Sakerin, S.M.; Macke, A.; Croot, P.; Zibordi, G.; et al. Maritime Aerosol Network as a component of Aerosol Robotic Network. *J. Geophys. Res.* **2009**, *114*, D06204. [CrossRef]
7. Takamura, T.; Nakajima, T. Overview of SKYNET and its activities. *Opt. Pura Apl.* **2004**, *37*, 3303–3308.
8. Pappalardo, G.; Amodeo, A.; Apituley, A.; Comeron, A.; Freudenthaler, V.; Linné, H.; Ansmann, A.; Bösenberg, J.; D'Amico, G.; Mattis, I.; et al. EARLINET: Towards an advanced sustainable European aerosol lidar network. *Atmos. Meas. Tech.* **2014**, *7*, 2389–2409. [CrossRef]
9. Welton, E.J.; Campbell, J.R.; Spinhirne, J.D.; Scott, V.S. Global monitoring of clouds and aerosols using a network of micro-pulse lidar systems. *Proc. SPIE* **2001**, *4153*, 151–158.
10. Sugimoto, N.; Nishizawa, T.; Shimizu, A.; Matsui, I.; Jin, Y. Characterization of aerosols in East Asia with the Asian Dust and aerosol lidar observation network (AD-Net). *Proc. SPIE* **2014**, *9262*, 92620K. [CrossRef]
11. Che, H.; Zhang, X.Y.; Chen, H.B.; Damiri, B.; Goloub, P.; Li, Z.Q.; Zhang, X.C.; Wei, Y.; Zhou, H.G.; Dong, F.; et al. Instrument calibration and aerosol optical depth validation of the China Aerosol Remote Sensing Network. *J. Geophys. Res.* **2009**, *114*, D03206. [CrossRef]
12. Dao, X.; Lin, Y.; Cao, F.; Di, S.; Hong, Y.; Xing, G.; Li, J.; Fu, P.; Zhang, Y. Introduction to the National Aerosol Chemical Composition Monitoring Network of China: Objectives, Current Status, and Outlook. *Bull. Am. Meteorol. Soc.* **2019**, *100*, ES337–ES351.
13. Laj, P.; Bigi, A.; Rose, C.; Andrews, E.; Lund Myhre, C.; Collaud Coen, M.; Lin, Y.; Wiedensohler, A.; Schulz, M.; Ogren, J.A.; et al. A global analysis of climate-relevant aerosol properties retrieved from the network of Global Atmosphere Watch (GAW) near-surface observatories. *Atmos. Meas. Tech.* **2020**, *13*, 4353–4392. [CrossRef]
14. Wielgosiński, G.; Czerwińska, J. Smog Episodes in Poland. *Atmosphere* **2020**, *11*, 277. [CrossRef]
15. Markowicz, K.M.; Chiliński, M.T.; Lisok, J.; Zawadzka, O.; Stachlewska, I.S.; Janicka, L.; Rozwadowska, A.; Makuch, P.; Pakszys, P.; Zieliński, T.; et al. Study of aerosol optical properties during long-range transport of biomass burning from Canada to Central Europe in July 2013. *J. Aerosol Sci.* **2016**, *101*, 156–173. [CrossRef]

16. Stachlewska, I.S.; Samson, M.; Zawadzka, O.; Harenda, K.M.; Janicka, L.; Poczta, P.; Szczepanik, D.; Heese, B.; Wang, D.; Borek, K.; et al. Modification of Local Urban Aerosol Properties by Long-Range Transport of Biomass Burning Aerosol. *Remote Sens.* **2018**, *10*, 412. [CrossRef]
17. Stachlewska, I.S.; Zawadzka, O.; Engelmann, R. Effect of Heat Wave Conditions on Aerosol Optical Properties Derived from Satellite and Ground-Based Remote Sensing over Poland. *Remote Sens.* **2017**, *9*, 1199. [CrossRef]
18. Papayannis, A.; Amiridis, V.; Mona, L.; Tsaknakis, G.; Balis, D.; Bösenberg, J.; Chaikovski, A.; De Tomasi, F.; Grigorov, I.; Mattis, I.; et al. Systematic lidar observations of Saharan dust over Europe in the frame of EARLINET (2000–2002). *J. Geophys. Res.* **2008**, *113*, D10204. [CrossRef]
19. Morys, M.; Mims, F.M.; Hagerup, S.; Anderson, S.E.; Baker, A.; Kia, J.; Walkup, T. Design, calibration, and performance of MICROTOPS II handheld ozone monitor and Sun photometer. *J. Geophys. Res.* **2001**, *106*, 14573–14582. [CrossRef]
20. Serrano, A.; Sanchez, G.; Cancillo, M.L. Correcting Daytime Thermal Offset in Unventilated Pyranometers. *J. Atmos. Ocean. Technol.* **2015**, *32*, 2088–2099. [CrossRef]
21. Michalsky, J.J.; Kutchenreiter, M.; Long, C.N. Significant Improvements in Pyranometer Nighttime Offsets Using High-Flow DC Ventilation. *J. Atmos. Ocean. Technol.* **2017**, *34*, 1323–1332. [CrossRef]
22. Markowicz, K.M.; Chiliński, M.T. Evaluation of Two Low-Cost Optical Particle Counters for the Measurement of Am-942 bient Aerosol Scattering Coefficient and Ångström Exponent. *Sensors* **2020**, *20*, 2617. [CrossRef]
23. Smirnov, A.; Holben, B.N.; Eck, T.F.; Dubovik, O. Cloud-screening and quality control algorithms for the AERONET database. *Remote Sens. Environ.* **2000**, *73*, 337–349. [CrossRef]
24. Alexandrov, M.D.; Marshak, A.; Cairns, B.; Lacis, A.A.; Carlson, B.E. Automated cloud screening algorithm for MFRSR data. *Geophys. Res. Lett.* **2004**, *31*, L04118. [CrossRef]
25. Justus, C.G.; Paris, M.V. A model for solar spectral irradiance and radiance at the bottom and top of a cloudless atmosphere. *J. Clim. Appl. Meteorol.* **1985**, *24*, 193–205. [CrossRef]
26. Müller, T.; Laborde, M.; Kassell, G.; Wiedensohler, A. Design and performance of a three-wavelength LED-based total scatter and backscatter integrating nephelometer. *Atmos. Meas. Tech.* **2011**, *4*, 1291–1303. [CrossRef]
27. Anderson, T.L.; Covert, D.S.; Marshall, S.F.; Laucks, M.L.; Charlson, R.J.; Waggoner, A.P.; Ogren, J.A.; Caldow, R.; Holm, R.L.; Quant, F.R.; et al. Performance characteristics of a high-sensitivity, three-wavelength, total scatter/backscatter nephelometer. *J. Atmos. Ocean. Technol.* **1996**, *13*, 967–986. [CrossRef]
28. Collaud Coen, M.; Weingartner, E.; Apituley, A.; Ceburnis, D.; Fierz-Schmidhauser, R.; Flentje, H.; Henzing, J.S.; Jennings, S.G.; Moerman, M.; Petzold, A.; et al. Minimizing light absorption measurement artifacts of the Aethalometer: Evaluation of five correction algorithms. *Atmos. Meas. Tech.* **2010**, *3*, 457–474. [CrossRef]
29. Baars, H.; Kanitz, T.; Engelmann, R.; Althausen, D.; Heese, B.; Komppula, M.; Preißler, J.; Tesche, M.; Ansmann, A.; Wandinger, U.; et al. An overview of the first decade of PollyNET: An emerging network of automated Raman-polarization lidars for continuous aerosol profiling. *Atmos. Chem. Phys.* **2016**, *16*, 5111–5137. [CrossRef]
30. Wang, D.; Stachlewska, I.S.; Delanoë, J.; Ene, D.; Song, X.; Schüttemeyer, D. Spatio-temporal discrimination of molecular, aerosol and cloud scattering and polarization using a combination of a Raman lidar, Doppler cloud radar and microwave radiometer. *Opt. Express* **2020**, *28*, 20117–20134. [CrossRef]
31. Freudenthaler, V. About the effects of polarising optics on lidar signals and the Δ90 calibration. *Atmos. Meas. Tech.* **2016**, *9*, 4181–4255. [CrossRef]
32. Engelmann, R.; Kanitz, T.; Baars, H.; Heese, B.; Althausen, D.; Skupin, A.; Wandinger, U.; Komppula, M.; Stachlewska, I.S.; Amiridis, V.; et al. The automated multiwavelength Raman polarization and water-vapor lidar PollyXT: The neXT generation. *Atmos. Meas. Tech.* **2016**, *9*, 1767–1784. [CrossRef]
33. Veselovskii, I.; Kolgotin, A.; Griaznov, V.; Müller, D.; Franke, K.; Whiteman, D.N. Inversion of multiwavelength Raman lidar data for retrieval of bimodal aerosol size distribution. *Appl. Opt.* **2004**, *43*, 1180–1195. [CrossRef] [PubMed]
34. Janicka, L.; Stachlewska, I.S.; Veselovskii, I.; Baars, H. Temporal variations in optical and microphysical properties of mineral dust and biomass burning aerosol derived from daytime Raman lidar observations over Warsaw, Poland. *Atmos. Environ.* **2017**, *169*, 162–174. [CrossRef]
35. Böckmann, C.; Mironova, I.; Müller, D.; Schneidenbach, L.; Nessler, R. Microphysical aerosol parameters from multiwavelength lidar. *J. Opt. Soc. Am.* **2005**, *22*, 518–528. [CrossRef]
36. Ortiz-Amezcua, P.; Guerrero-Rascado, J.L.; Granados-Muñoz, M.J.; Benavent-Oltra, J.A.; Böckmann, C.; Samaras, S.; Stachlewska, I.S.; Janicka, Ł.; Baars, H.; Bohlmann, S.; et al. Microphysical characterization of long-range transported biomass burning particles from North America at three EARLINET stations. *Atmos. Chem. Phys.* **2017**, *17*, 5931–5946. [CrossRef]
37. Stachlewska, I.S.; Costa-Suros, M.; Althausen, D. Raman lidar water vapor profiling over Warsaw, Poland. *Atmos. Res.* **2017**, *194*, 258–267. [CrossRef]
38. Wang, D.; Stachlewska, I.S.; Song, X.; Heese, B.; Nemuc, A. Variability of the Boundary Layer Over an Urban Continental Site Based on 10 Years of Active Remote Sensing Observations in Warsaw. *Remote Sens.* **2020**, *12*, 340. [CrossRef]
39. Stachlewska, I.; Piądłowski, M.; Migacz, S.; Szkop, A.; Zielińska, A.; Swaczyna, P. Ceilometer observations of the boundary layer over Warsaw, Poland. *Acta Geophys.* **2012**, *60*, 1386–1412. [CrossRef]
40. Szczepanik, D.; Stachlewska, I.S.; Tetoni, E.; Althausen, D. Properties of Saharan Dust versus Local Urban Dust—A case study. *Earth Space Sci.* **2021**, *8*, e2021EA001816. [CrossRef]

41. Berk, A.; Anderson, G.P.; Acharya, P.K.; Bernstein, L.S.; Muratov, L.; Lee, J.; Fox, M.J.; Adler-Golden, S.M.; Chetwynd, J.H.; Hoke, M.L.; et al. MODTRAN5: A reformulated atmospheric band model with auxiliary species and practical multiple scattering options, Proc. SPIE 5655. *Multispectr. Hyperspectr. Remote Sens. Instrum. Appl. II* **2005**, *5655*, 88–95. [CrossRef]
42. Fu, Q.; Liou, K.N. On the correlated k-distribution method for radiative transfer in nonhomogeneous atmospheres. *J. Atmos. Sci.* **1992**, *49*, 2139–2156. [CrossRef]
43. Conant, W.C. An observational approach for determining aerosol surface radiative forcing: Results from the first field phase of INDOEX. *J. Geophys. Res.* **2000**, *105*, 15347–15360. [CrossRef]
44. Karlsson, K.-G.; Anttila, K.; Trentmann, J.; Stengel, M.; Fokke Meirink, J.; Devasthale, A.; Hanschmann, T.; Kothe, S.; Jääskeläinen, E.; Sedlar, J.; et al. CLARA-A2: The second edition of the CM SAF cloud and radiation data record from 34 years of global AVHRR data. *Atmos. Chem. Phys.* **2017**, *17*, 5809–5828. [CrossRef]
45. Markowicz, K.M.; Ritter, C.; Lisok, J.; Makuch, P.; Stachlewska, I.S.; Cappelletti, D.; Mazzola, M.; Chilinski, M.T. Vertical variability of aerosol single-scattering albedo and black carbon concentration based on in-situ and remote sensing techniques during iAREA campaigns in Ny-Ålesund. *Atmos. Environ.* **2017**, *164*, 431–447. [CrossRef]
46. Markowicz, K.M.; Zawadzka, O.; Lisok, J.; Chilinski, M.T.; Xian, P. Impact of moderate absorbing aerosol on surface sensible, latent and net radiative fluxes during summer of 2015 over Central Europe. *J. Aerosol Sci.* **2020**, *151*, 105627. [CrossRef]
47. Zieliński, T.; Petelski, T.; Makuch, P.; Strzałkowska, A.; Ponczkowska, A.; Markowicz, K.M.; Chourdakis, G.; Georgoussis, G.; Kratzer, S. Studies of Aerosols Advected to Coastal Areas with the Use of Remote Techniques. *Acta Geophys.* **2012**, *60*, 1359–1385. [CrossRef]
48. Zawadzka, O.; Makuch, P.; Markowicz, K.M.; Zieliński, T.; Petelski, T.; Ulevicius, V.; Strzałkowska, A.; Rozwadowska, A.; Gutowska, D. Studies of Aerosol Optical Depth with the Use of Microtops II Sun Photometers and MODIS Detectors in Coastal Areas of the Baltic Sea. *Acta Geophys.* **2014**, *62*, 400–422. [CrossRef]
49. Zawadzka, O.; Markowicz, K.M. Retrieval of Aerosol Optical Depth from Optimal Interpolation Approach Applied to SEVIRI Data. *Remote Sens.* **2014**, *6*, 7182–7211. [CrossRef]
50. Krówczyńska, M.; Wilk, E.; Pabjanek, P.; Zagajewski, B.; Meuleman, K. Mapping asbestos-cement roofing with the use of APEX hyperspectral airborne imagery: Karpacz area, Poland—A case study. *Misc. Geogr.* **2016**, *20*, 41–46. [CrossRef]
51. Chiliński, M.T.; Markowicz, K.M.; Zawadzka, O.; Stachlewska, I.S.; Kumala, W.; Petelski, T.; Makuch, P.; Westphal, D.L.; Zagajewski, B. Modelling and observation of mineral dust optical properties over Central Europe. *Acta Geophys.* **2016**, *64*, 2550–2590. [CrossRef]
52. Markuszewski, P.; Petelski, T.; Zielinski, T. Marine aerosol fluxes determined by simultaneous measurements of eddy covariance and gradient method. *Environ. Eng. Manag. J.* **2018**, *17*, 261–265. [CrossRef]
53. Makuch, P.; Sitarek, S.; Markuszewski, P.; Petelski, T.; Stacewicz, T. Lidar observation of aerosol transformation in the atmospheric boundary layer above the Baltic Sea. *Oceanologia* **2021**, *63*, 238–246. [CrossRef]
54. Chilinski, M.T.; Markowicz, K.M.; Markowicz, J. Observation of vertical variability of black carbon concentration in lower troposphere on campaigns in Poland. *Atmos. Environ.* **2016**, *137*, 155–170. [CrossRef]
55. Chilinski, M.T.; Markowicz, K.M.; Kubicki, M. UAS as a support for atmospheric aerosols research. *Pure Appl. Geophys.* **2018**, *175*, 3325–3342. [CrossRef]
56. Zawadzka, O.; Posyniak, M.; Nelken, K.; Markuszewski, P.; Chiliński, M.T.; Czyżewska, D.; Lisok, J.; Markowicz, K.M. Study of the vertical variability of the aerosol properties based on cable cars in-situ measurements. *Atmos. Pollut. Res.* **2017**, *8*, 968–978. [CrossRef]
57. Posyniak, M.; Markowicz, K.M.; Czyżewska, D.; Chiliński, M.; Makuch, P.; Zawadzka-Manko, O.; Kucięba, S.; Kulesza, K.; Kachniarz, K.; Mijal, K.; et al. Experimental study of smog microphysical and optical vertical structure in the mountain area—Poland. *J. Pollut. Res.* **2021**, *12*, 101171. [CrossRef]
58. Wang, D.; Szczepanik, D.; Stachlewska, I.S. Interrelations between surface, boundary layer, and columnar aerosol properties over a continental urban site. *Atmos. Chem. Phys.* **2019**, *19*, 13097–13128. [CrossRef]
59. Wang, D.; Stachlewska, I.S. Stratospheric Smoke Properties Based on Lidar Observations in Autumn 2017 Over Warsaw. *EPJ Web Conf.* **2020**, *237*, 02033. [CrossRef]
60. Markowicz, K.M.; Zawadzka-Manko1, O.; Posyniak, M. A large reduction of direct aerosol cooling over Poland in the last decades. *Int. J. Climatol.* **2021**.
61. Posyniak, M.; Szkop, A.; Pietruczuk, A.; Podgórski, J.; Krzyścin, J. The Long-Term (1964–2014) Variability of Aerosol Optical Thickness and its Impact on Solar Irradiance Based on the Data Taken at Belsk, Poland. *Acta Geophys.* **2016**, *64*, 1858–1874. [CrossRef]
62. Markowicz, K.M.; Zawadzka, O.; Posyniak, M.; Uscka-Kowalkowska, J. Long-term variability of aerosol optical depth in the Tatra Mountains region of the Central Europe. *J. Geophys. Res.* **2019**, *124*, 3464–3475. [CrossRef]
63. Markowicz, K.M.; Uscka-Kowalkowska, J. Long-term and seasonal variability of the aerosol optical depth at Mt. Kasprowy Wierch (Poland). *J. Geophys. Res.* **2015**, *120*, 1865–1879. [CrossRef]
64. Chiliński, M.T.; Markowicz, K.M.; Zawadzka, O.; Stachlewska, I.S.; Lisok, J.; Makuch, P. Comparison of columnar, surface and UAS profiles of absorbing aerosol optical depth and single scattering albedo. *Atmosphere* **2019**, *10*, 446. [CrossRef]

65. Harenda, K.M.; Samson, M.; Juszczak, R.; Markowicz, K.M.; Stachlewska, I.S.; Kleniewska, M.; MacArthur, A.; Schüttemeyer, D.; Chojnicki, B.H. Impact of Atmospheric Optical Properties on Net Ecosystem Productivity of Peatland in Poland. *Remote Sens.* **2021**, *13*, 2124. [CrossRef]
66. Pietruczuk, A.; Chaikovsky, A. Variability of aerosol properties during the 2007–2010 spring seasons over central Europe. *Acta Geophys.* **2012**, *60*, 1338–1358. [CrossRef]
67. Szczepanik, D.; Markowicz, K.M. The relation between columnar and surface aerosol optical properties in a background environment. *Atmos. Pollut. Res.* **2018**, *9*, 246–256. [CrossRef]
68. Zawadzka, O.; Markowicz, K.M.; Pietruczuk, A.; Zielinski, T.; Jarosławski, J. Impact of urban pollution emitted in Warsaw on aerosol properties. *Atmos. Environ.* **2013**, *69*, 15–28. [CrossRef]
69. Sokół, P.; Stachlewska, I.S.; Ungureanu, I.; Stefan, S. Evaluation of the Boundary Layer Morning Transition Using the CL-31 Ceilometer Signals. *Acta Geophys.* **2014**, *62*, 367–380. [CrossRef]
70. Petelski, T. Marine aerosol fluxes over open sea calculated from vertical concentration gradients. *J. Aerosol Sci.* **2003**, *34*, 359–371. [CrossRef]
71. Petelski, T.; Markuszewski, P.; Makuch, P.; Jankowski, A.; Rozwadowska, A. Studies of vertical coarse aerosol fluxes in the boundary layer over the Baltic Sea. *Oceanologia* **2014**, *56*, 697–710. [CrossRef]
72. Markuszewski, P.; Kosecki, S.; Petelski, T. Sea spray aerosol fluxes in the Baltic Sea region: Comparison of the WAM model with measurements. *Estuar. Coast. Shelf Sci.* **2017**, *195*, 16–22. [CrossRef]
73. Massel, S.R. Chapter 9 Marine aerosol fluxes. In *Ocean Waves Breaking and Marine Aerosol Fluxes*; Springer: New York, NY, USA, 2007; p. 229e246.
74. Nilsson, E.D.; Rannik, Ü.; Swietlicki, E.; Leck, C.; Aalto, P.P.; Zhou, J.; Norman, M. Turbulent aerosol fluxes over the Arctic Ocean: 2. Wind-driven sources from the sea. *J. Geophys. Res. Atmos.* **2001**, *106*, 32139–32154. [CrossRef]
75. Nilsson, E.D.; Hultin, K.A.; Mårtensson, E.M.; Markuszewski, P.; Rosman, K.; Krejci, R. Baltic Sea Spray Emissions: In Situ Eddy Covariance Fluxes vs. Simulated Tank Sea Spray. *Atmosphere* **2021**, *12*, 274. [CrossRef]
76. Markuszewski, P.; Klusek, Z.; Nilsson, E.D.; Petelski, T. Observations on relations between marine aerosol fluxes and surface-generated noise in the southern Baltic Sea. *Oceanologia* **2020**, *62*, 413–427. [CrossRef]
77. Kaminski, J.W.; Neary, L.; Struzewska, J.; McConnell, J.C.; Lupu, A.; Jarosz, J.; Toyota, K.; Gong, S.L.; Liu, X.; Chance, K.; et al. GEM-AQ, an on-line global multiscale chemical weather modelling system: Model description and evaluation of gas phase chemistry processes. *Atmos. Chem. Phys.* **2008**, *8*, 3255–3281. [CrossRef]
78. Struzewska, J.; Kaminski, J.W.; Jefimow, M. Application of model output statistics to the GEM-AQ high resolution air quality forecast. *Atmos. Res.* **2016**, *181*, 186–199. [CrossRef]
79. Werner, M.; Kryza, M.; Guzikowski, J. Can data assimilation of surface PM2.5 and Satellite AOD improve WRF-Chem Forecasting? A case study for two scenarios of particulate air pollution episodes in Poland. *Remote Sens.* **2019**, *11*, 2364. [CrossRef]
80. Lynch, P.; Reid, J.S.; Westphal, D.L.; Zhang, J.; Hogan, T.F.; Hyer, E.J.; Curtis, C.A.; Hegg, D.A.; Shi, Y.; Campbell, J.R.; et al. An 11-year global gridded aerosol optical thickness reanalysis (v1.0) for atmospheric and climate sciences. *Geosci. Model Dev.* **2017**, *9*, 1489–1522. [CrossRef]
81. Markowicz, K.M.; Flatau, P.J.; Remiszewska, J.; Witek, M.; Reid, E.A.; Reid, J.S.; Bucholtz, A.; Holben, B. Observations and Modeling of the Surface Aerosol Radiative Forcing during UAE^2. *J. Atmos. Sci.* **2008**, *65*, 2877–2891. [CrossRef]